# Supporting Information

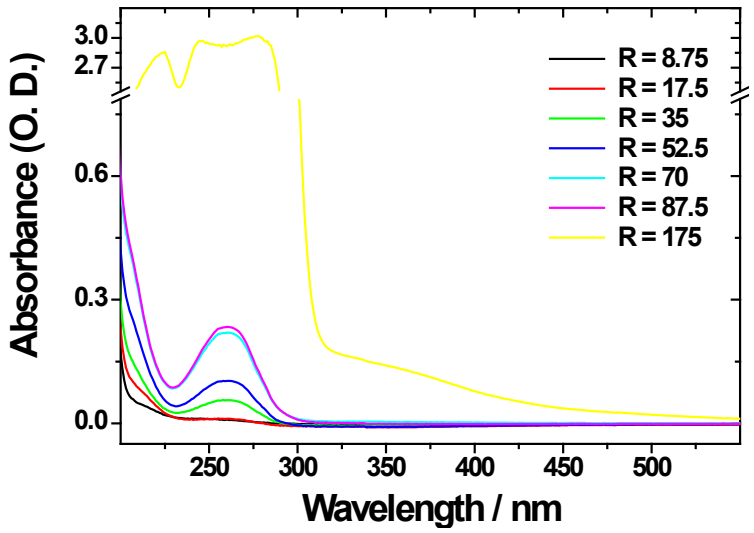


**Figure S1.** UV-visible spectra of the supernatants after complexation of Li28 with iron oxide nanoparticles for the different values of *R*.

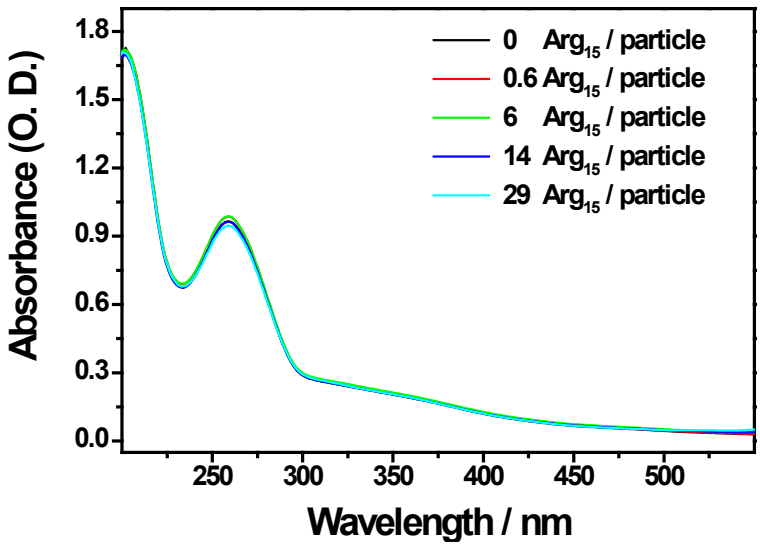


**Figure S2.** UV-visible spectra of the supernatants after complexation ("step by step") of Li28 and $Arg_{15}$ with iron oxide nanoparticles for the different amounts of $Arg_{15}$.

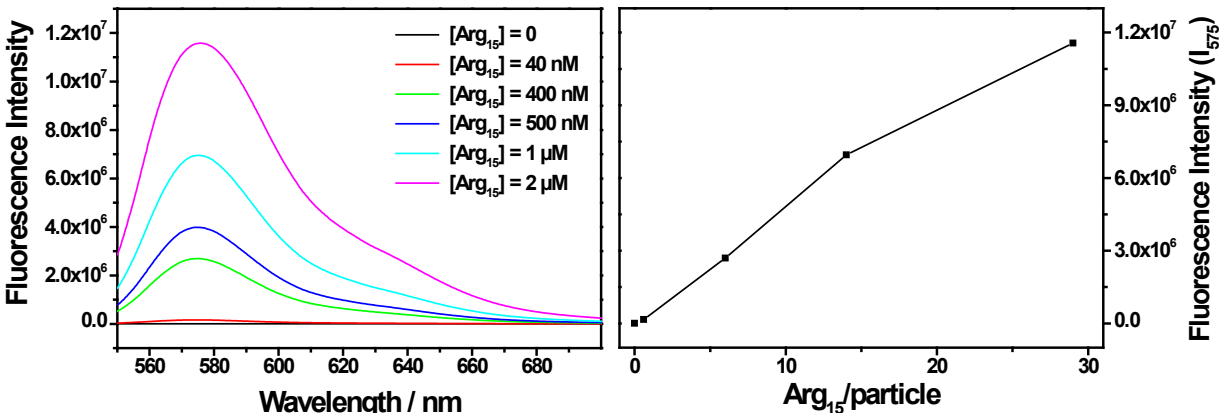


**Figure S3.** Fluorescence spectra of the TAMRA-labeled $Arg_{15}$ and calibration curve.

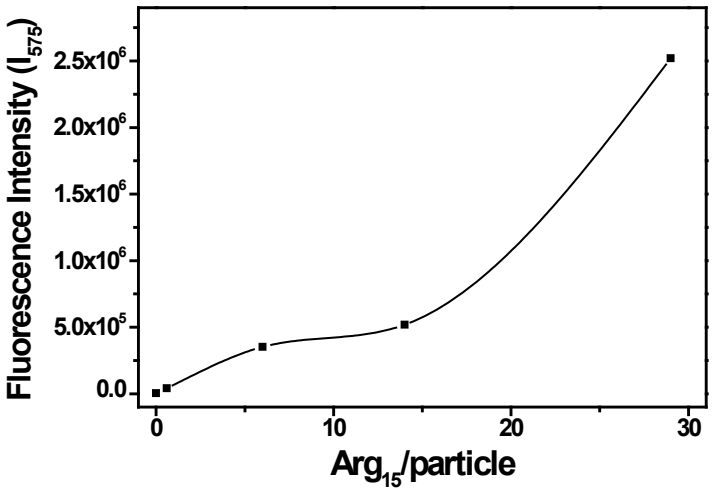


**Figure S4.** Fluorescence spectra of the supernatants after complexation ("step by step") of Li28 and $Arg_{15}$ with iron oxide nanoparticles for the different amounts of $Arg_{15}$.

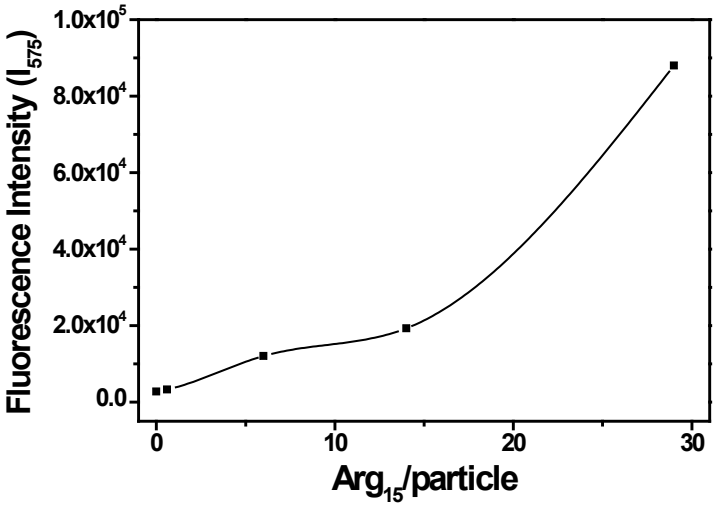


**Figure S5.** Fluorescence spectra of the complexes (complexation "step by step") of Li28 and $Arg_{15}$ with iron oxide nanoparticles for the different amounts of $Arg_{15}$.

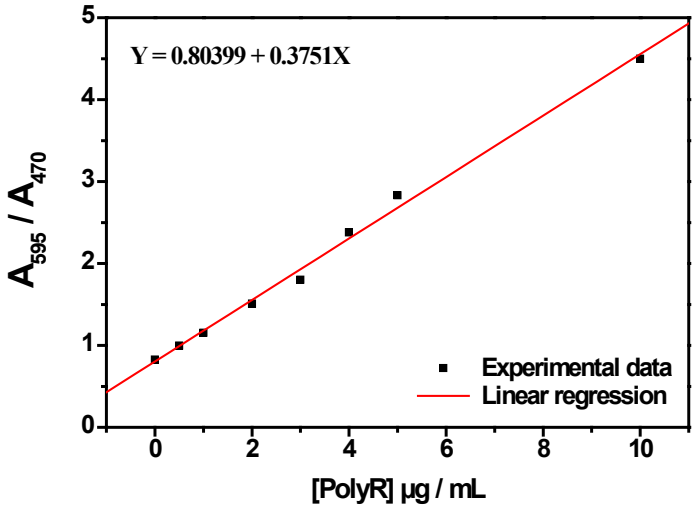


**Figure S6.** Calibration curve of the Bradford PolyR assay.

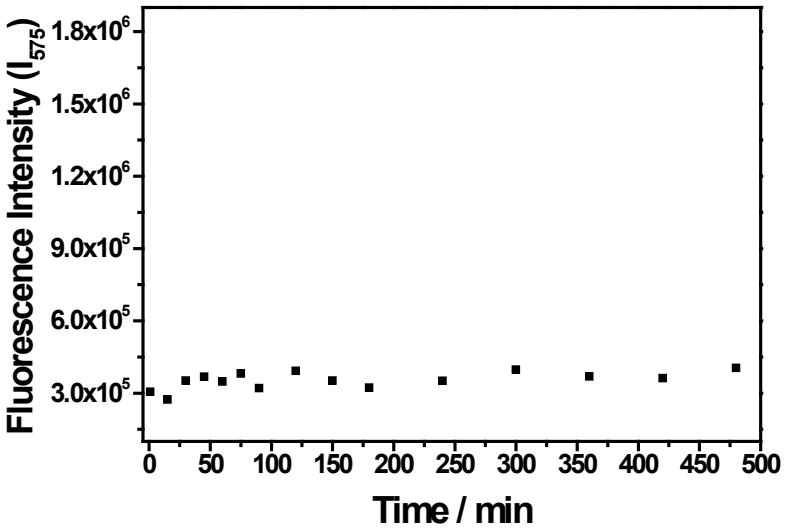


**Figure S7.** Fluorescence intensity of the nanocomplex in the presence of 10% serum.

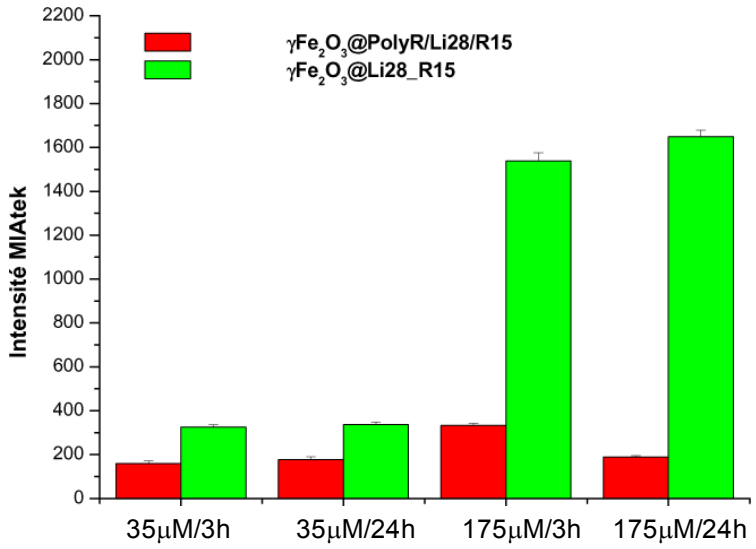


**Figure S8.** Intracellular internalisation of NPs was quantified with the MIAtek kit, 3 h after incubation with the NPs, and after a subsequent 24-h wash-out period.

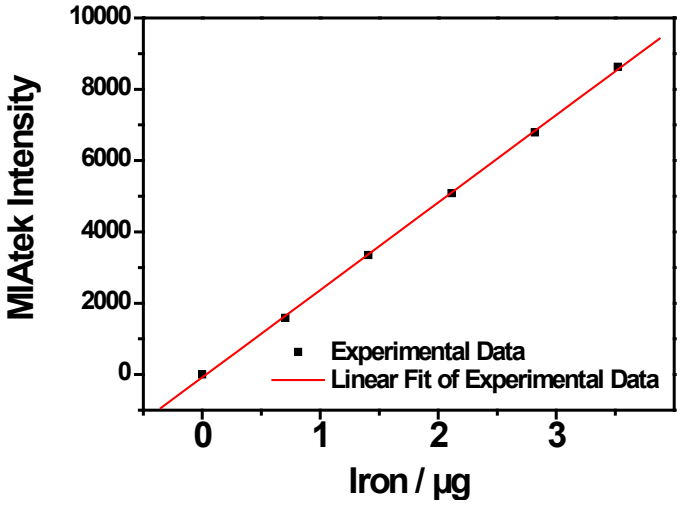


**Figure S9.** Calibration curve used for the MIAtek quantification.

**Table S1.** Percentage yield of complexation of Li28 with iron oxide nanoparticles for the different values of *R*.

| Values | ***R*** | | | | | | |
|---|---|---|---|---|---|---|---|
| | **8.75** | **17.5** | **35** | **52.5** | **70** | **87.5** | **175** |
| **Yield %** | 98.3 | 98.9 | 98 | 98.1 | 95.9 | 96.7 | - |
| **Li28/particle** | 8.6 | 17.3 | 34.3 | 51.2 | 67.1 | 84.6 | - |

**Table S2.** Percentage yield of complexation of $Arg_{15}$ (complexation "step by step").

| Values | **($Arg_{15}$/Particle)** | | | | |
|---|---|---|---|---|---|
| | **0** | **0.6** | **6** | **14** | **29** |
| **Yield %** | - | 74 | 87 | 92 | 78 |
| **$Arg_{15}$/particle** | - | 0.4 | 5 | 13 | 23 |